

Islanding detection in three-phase and single-phase systems using pulsating high frequency signal injection

David Reigosa, Fernando Briz, Cristian Blanco, Juan Manuel Guerrero
University of Oviedo. Dept. of Elect., Computer & System Engineering, Gijón, 33204, Spain.
reigosa@isa.uniovi.es, fernando@isa.uniovi.es, blancocristian@uniovi.es, guerrero@isa.uniovi.es

Abstract: This paper analyzes the use of pulsating high frequency signal injection for islanding detection purposes. Active islanding detection using high frequency signal injection is an appealing option due to its reduced non-detection zone, reduced cost and ease of implementation. The use of a rotating high frequency signal has been reported and analyzed. However, this method can only be applied to three-phase systems. In this paper, the use of a pulsating high frequency signal injection is proposed. While it uses the same principles as rotating signal injection, it can be applied to both three-phase and single-phase systems.¹

I. Introduction

Islanding is defined as the situation where a distributed generator (DG) or DGs continue generating power when they are not connected to the utility grid. Islanding detection has been the focus of significant research efforts during the last years due to the increasing share of the distributed generation in the power system. Distributed generation can be based either on renewable (wind turbines, photovoltaic, ...) and non-renewable (biomass, fuel cells, micro-gas turbines, ...) energy resources. National, regional and local authorities regulate the interconnection of the distributed energy resources to the utility grid, in most of the cases following the standards and recommendation that are published by standardizing institutions [1-8]. In all the cases the standards require that the system has to detect if it is connected or disconnected from the utility grid (islanding detection) within a timeframe, e.g. 2 seconds for the IEEE-1547 [1], UL-1741 [2], IEC-62116 [3], AS-4777 [4], IEEE-929 [5] and DIN-VDE-0126 [6], or 5 seconds for the Swiss [7] and Australian [8] standards. These standards use the impedance variation within the considered timeframe as the metric for islanding detection, e.g. 1 Ω variation for the German and 0.5 Ω for the Swiss and Australian.

Three different scenarios can be considered for islanding detection: *Single-inverter*, *Multi-inverter* and *Microgrid* [9]. In the *Single-inverter* scenario only one DG exists and all the power is exported to the grid. In the *Multi-inverter* scenario most (or all) of the power generated by the DGs is exported to the grid throughout the point of common coupling (PCC). In the *Microgrid* scenario, a major portion (or all) of power generated by the DGs is consumed by the microgrid loads, the remaining power being exported to the grid throughout the PCC. The *Multi-inverter* case could be considered as a particular case of the *Microgrid* scenario, but with a major portion of the energy being exported to the utility grid. In all cases, the system is required to have the ability to detect if it is connected or isolated from the utility grid [9, 17-19].

Islanding detection methods can be classified into three groups: passive [10, 11], active [9, 11-19] and

communication based [11] methods. Passive and active methods are inverter resident [9, 10], while communication based methods are remote [9, 10]. Passive based methods are grid friendly, as they do not introduce any disturbance in the grid [10], but have the disadvantage of a large non-detection-zone (NDZ) [11]. Active methods are based on the injection of some disturbing signal in the grid [9, 11-19], therefore having a negative impact on the power quality. However, they have low NDZ [17, 18], being easy and cheap to implement. Finally, communication based methods have no NDZ, but they need a communication infrastructure, being therefore subjected to communication failures [10, 17, 18].

Active islanding detection based methods can be further divided into two groups:

- Grid variable variation based methods [11]. Islanding is detected from the grid response to a small disturbance, typically in the voltage or frequency, produced by the power converter connecting the DG to the microgrid.
- Impedance estimation based methods [11-19]. In these methods, islanding is detected from variations at the power converter output impedance. These methods can be further divided into methods that estimate the impedance by the variation of the active/reactive power [12] or by the injection of some form of high frequency excitation [13-18]. The high frequency excitation can be injected continuously or intermittently [17, 18]. The use of harmonics due to the non-ideal behavior of PWM inverters has also been recently proposed to estimate the high frequency impedance [19], no high frequency signal being injected in this case.

While the implementation of islanding active method based on the high frequency impedance variation is relatively simple in the case of *Single-inverter*, interference among converters can occur both in the *Multi-inverter* and *Microgrid* scenarios, which can result in erroneous impedance estimation and therefore incorrect islanding detection [9, 17, 18]. Strategies to prevent from this to happen have already been proposed [9, 18].

Most of the impedance estimation active islanding detection methods that have been proposed are intended for three-phase systems [11-18]. Nevertheless, single-phase DGs (e.g. single-phase micro-wind generation, small-scale solar panel, ...) for low-power home applications are becoming of great interest. The reduced implementation cost of the active islanding detection based methods therefore makes them an appealing option for these kinds of applications.

In this paper, islanding detection using a pulsating high frequency signal is proposed. The main advantage of the pulsating excitation compared to other forms of high frequency excitations that have already been proposed is that it can be used indistinctly with single-phase and three-phase systems.

¹ This work was supported in part by the Research, Technological Development and Innovation Programs of the Ministry of Science and Innovation under grant MICINN-10-CSD2009-00046 and by the Personnel Research Training Program funded by the Regional Ministry of Education and Science of the Principality of Asturias under grant BP11-107.

The paper is organized as follows. A brief review of active islanding detection methods based on high frequency signal injection as well as the analytical formulation of the proposed method is presented in section II. The use of pulsating high frequency signal injection for phase-to-phase and phase-to-ground fault detection in three-phase systems is discussed in Section III. Finally simulation and experimental results confirming the viability of the method are shown in section IV and V respectively.

II. Islanding detection using pulsating high frequency signal injection

DGs are usually connected to the main grid/microgrid by means of a three-phase (see Fig. 1a) or single-phase (see Fig. 1b) PWM-VSI [17-20]. The H-bridge inverter (Fig. 1b) is the most common topology in single-phase systems [20]. High frequency signal injection active islanding detection based methods inject a high frequency signal superposed on the fundamental voltage through the PWM-VSIs, islanding being detected from the variations of the measured high frequency impedance. The use of a rotating high frequency signal has been proposed for islanding detection [9, 17-19]; however this type of high frequency excitation cannot be applied to single-phase systems.

Selection of the frequency for the high frequency excitation involves trading off several issues, including the adverse impact of the injected signal on the power quality, the spectral separation with the fundamental voltage as well as with the output LCL filter and the grid resonance frequencies [17, 18]. Frequencies ranging between 75 and 400 Hz can be found in the literature [9, 11-19].

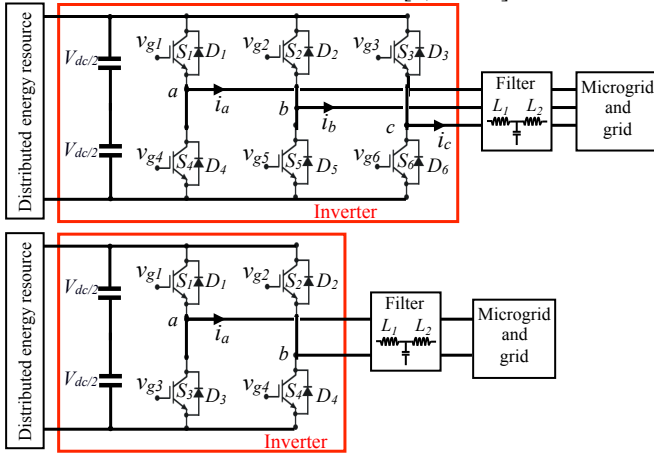


Fig 1. Simplified distributed energy resource connection to the utility/grid/microgrid using a) a three-phase VSI, and b) a single-phase VSI.

The principles and implementation of the proposed islanding detection method using a pulsating high frequency signal are analyzed following. In the first place, the case of three-phase system is considered, the single-phase case being analyzed later.

a) Three-phase systems

When a pulsating high frequency signal voltage (1) is injected into a three-phase system with an angle of injection φ_i , the resulting high frequency current at the output of the LCL filter (see Fig. 1) is given by (2), the grid high frequency impedance being (3), where v_{dqhf} is the injected

high frequency voltage complex vector, V_{hf} is the magnitude of the injected high frequency signal, ω_{hf} is the frequency of the high frequency signal, $v_{dq\mu g hf}$ is the output LCL filter high frequency voltage complex vector, $i_{dq\mu g hf}$ is the output LCL filter high frequency current complex vector, i_{dqhf} is the output inverter high frequency current complex vector, L_1 is the inverter side LCL filter inductance, L_2 is the grid side LCL filter inductance, $Z_{dq\mu g hf}$ is the microgrid high frequency impedance and φ_z is the phase of the microgrid high frequency impedance. The transformation from three-phase to $dq0$ quantities is given by (4). The angle of injection φ_i can be selected to be constant, or can change with an angular frequency of ω_i . In the first case, the pulsating signal will be injected in a stationary reference frame, while in the second case, the pulsating signal is injected in a reference frame that rotates at ω_i .

It is observed from (1)-(2) that the pulsating high frequency voltage and current can be decomposed into two rotating signals ($v_{dqhf}^{pc}, v_{dqhf}^{nc}, i_{dqhf}^{pc}, i_{dqhf}^{nc}$) which rotate in opposite direction, each of half the amplitude of the injected signal. Both components can potentially be used for high frequency impedance estimation (3).

$$v_{dqhf} = V_{hf} \cos(\omega_{hf} t) e^{j\varphi_i} = V_{hf} \cos(\omega_{hf} t) e^{j\omega_i t} = \frac{V_{hf}}{2} e^{j(\omega_{hf} + \omega_i)t} + \frac{V_{hf}}{2} e^{j(-\omega_{hf} + \omega_i)t} = v_{dqhf}^{pc} + v_{dqhf}^{nc} \quad (1)$$

$$i_{dq\mu g hf} = \frac{v_{dqhf} - v_{dq\mu g hf} - j\omega_{hf} L_1 i_{dqhf}}{j\omega_{hf} L_2} = \frac{V_{hf}}{2 * |Z_{dq\mu g hf}|} e^{j((\omega_{hf} + \omega_i)t - \varphi_z)} + \frac{V_{hf}}{2 * |Z_{dq\mu g hf}|} e^{j((- \omega_{hf} + \omega_i)t + \varphi_z)} = i_{dq\mu g hf}^{pc} + i_{dq\mu g hf}^{nc} \quad (2)$$

$$Z_{dqhf \mu g} = \frac{v_{dq\mu g hf}^{pc}}{i_{dq\mu g hf}^{pc}} = \frac{v_{dq\mu g hf}^{nc}}{i_{dq\mu g hf}^{nc}} = \frac{e^{j((\omega_{hf} + \omega_i)t)} V_{hf} / 2}{e^{j((\omega_{hf} + \omega_i)t - \varphi_z)} * V_{hf} / 2 * |Z_{dq\mu g hf}|} = \frac{e^{j((- \omega_{hf} + \omega_i)t)} V_{hf} / 2}{e^{j((- \omega_{hf} + \omega_i)t + \varphi_z)} * V_{hf} / 2 * |Z_{dq\mu g hf}|} \quad (3)$$

$$f_{dq} = 2/3(f_a + f_b e^{j*2*\pi/3} + f_c e^{j*4*\pi/3}) e^{-j*\varphi_i} \quad (4)$$

$$f_0 = 1/3(f_a + f_b + f_c)$$

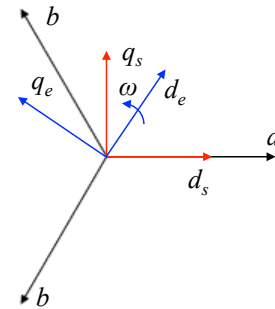


Fig. 2 abc and dq reference systems. dq_s =stationary reference frame,

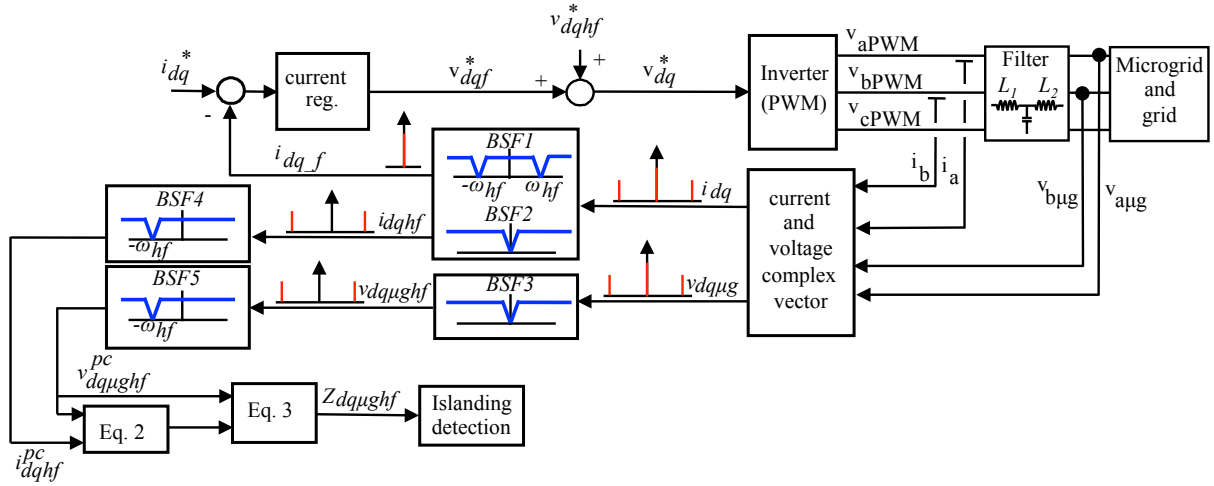


Fig 3. Signal processing for islanding detection using a three-phase inverter.

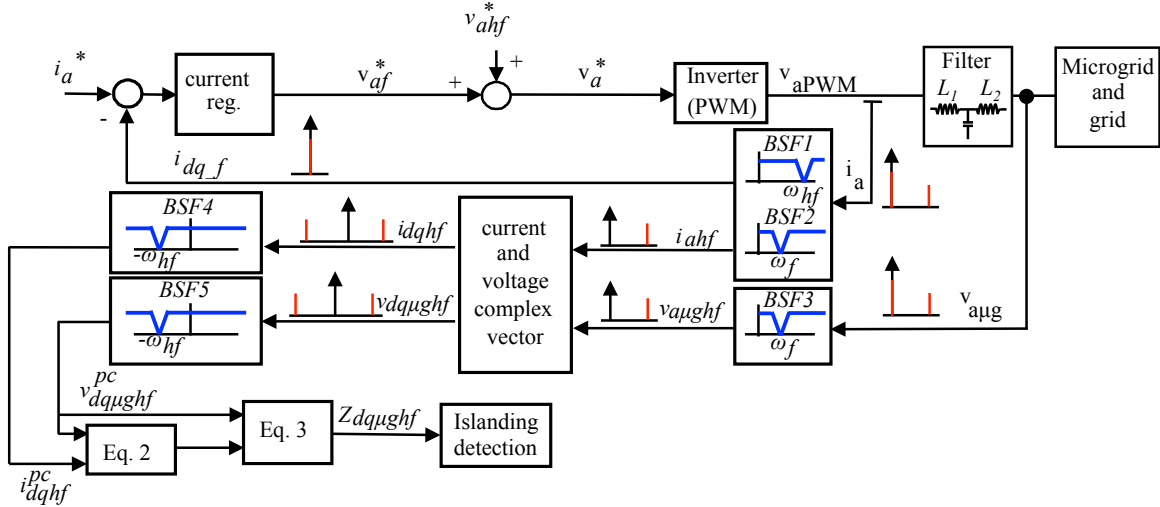


Fig 4. Signal processing for islanding detection using a single-phase inverter.

dq_e =rotating reference frame.

In the discussion following, it is assumed that the neutral of the loads are connected to ground, which is the case for low voltage public distribution systems [22]. However, the neutral wire is not typically available in the connection of three-phase distributed energy resources to the utility grid/microgrid through three-phase VSI (see Fig. 1a). Therefore the zero sequence component of the current (4) is always zero in the inverter side.

The pulsating high frequency signal can be injected either in a stationary reference frame ($\omega_i=0$ in (1), see dq_s in Fig. 2) or in a rotating reference frame ($\omega_i \neq 0$ in (1), see dq_e in Fig. 2). When the high frequency signal is injected in a reference frame that rotates e.g. aligned with the d_e or q_e axis (see Fig. 2), all the phases are excited sequentially, meaning that the high frequency impedance of all the three phases can be measured. On the contrary, if the high frequency signal is injected in a stationary reference frame, one, two or all the three phases can be excited, depending on the angle of injection selected. As an example, only phase a is excited if the signal is injected in the d_s axis, (see Fig. 2), in this case the high frequency signal will be sensitive only to phase a condition. It is also noted that since the connection/disconnection between the microgrid and the grid occurs simultaneously in all the three phases, the number of

phases being excited would be irrelevant for islanding detection, i.e. all the three phases reflect the island-grid transitions. However, sequential excitation of all phases opens interesting possibilities for detecting asymmetric faults in three phase systems. This issue will be discussed in detail in section III.

Fig. 3 shows the signal processing needed for islanding detection using a pulsating high frequency signal for the case of a three-phase system. In the implementation shown in Fig. 3 the PWM-VSI is current regulated. In this case, the current regulator can react against the induced high frequency current. To prevent this, band-stop filters are used to reject the positive and negative sequence current components (2) from the current feedback ($BSF1$ in Fig. 3). Band-stop filters $BSF2$ and $BSF3$ in Fig. 3 are used to reject the fundamental component of the voltage and current respectively, while $BSF4$ and $BSF5$ reject the negative sequence components, the positive sequence component of these signals being finally obtained. The high frequency impedance is obtained using (2) and (3), islanding being detected from the high frequency impedance variation.

b) Single-phase system

Though the concept of complex vector defined by (4) is only valid in principle for the case of three-phase systems, it is also possible to use it with single-phase systems. This can

be done by defining a complex vector in which one of the components (e.g. d -axis in (5) and (6)) is made equal to the corresponding single-phase voltage/current and the other component (e.g. q -axis in (5) and (6)) is made equal to zero. By doing this, the high frequency impedance (3) in a single-phase system can be estimated from (5) and (6), where v_{ahf} is the injected high frequency phase voltage, $v_{a\mu ghf}$ and $i_{a\mu ghf}$ are the LCL filter high frequency output phase voltage and current respectively and i_{ahf} is the inverter high frequency output phase current.

$$\begin{aligned}
 v_{dqhf} &= \begin{bmatrix} v_{ahf} \\ 0 \end{bmatrix} = \begin{bmatrix} V_{hf} \cos(\omega_{hf} t) \\ 0 \end{bmatrix} = \\
 &= \frac{V_{hf}}{2} e^{j\omega_{hf} t} + \frac{V_{hf}}{2} e^{-j\omega_{hf} t} = v_{dqhf}^{pc} + v_{dqhf}^{nc} \\
 i_{dq\mu ghf} &= \begin{bmatrix} i_{a\mu ghf} \\ 0 \end{bmatrix} = \begin{bmatrix} \frac{v_{ahf} - v_{a\mu ghf} - j\omega_{hf} L_1 i_{ahf}}{j\omega_{hf} L_2} \\ 0 \end{bmatrix} = \\
 &= \frac{V_{hf}}{2^* |Z_{dq\mu ghf}|} e^{j(\omega_{hf} t - \phi_2)} + \frac{V_{hf}}{2^* |Z_{dq\mu ghf}|} e^{j(-\omega_{hf} t + \phi_2)} = \\
 &= i_{dq\mu ghf}^{pc} + i_{dq\mu ghf}^{nc}
 \end{aligned} \quad (5)$$

$$\begin{aligned}
 &= \frac{V_{hf}}{2^* |Z_{dq\mu ghf}|} e^{j(\omega_{hf} t - \phi_2)} + \frac{V_{hf}}{2^* |Z_{dq\mu ghf}|} e^{j(-\omega_{hf} t + \phi_2)} = \\
 &= i_{dq\mu ghf}^{pc} + i_{dq\mu ghf}^{nc}
 \end{aligned} \quad (6)$$

Fig. 4 shows the signal processing needed for islanding detection in a single-phase system. A single band-stop filter is needed to reject the component at ω_{hf} (BSF1, see Fig. 4) to prevent the fundamental current regulator reaction. As for the three-phase system case, band-stop filters *BSF2* and *BSF3* reject the fundamental components and *BSF4* and *BSF5* reject the negative sequence components. Once the positive sequence component of the voltage and current are isolated, the high frequency impedance is obtained using (2) and (3), islanding being detected from the high frequency impedance variation.

It is finally noted that though in all the discussion presented in this paper it is assumed that a high frequency voltage is injected, it is possible to combine high frequency voltage injection and high frequency current injection as described in [9]. These can be advantageous when multiple parallel-connected inverters implement the method [9]. It is also noted that the dead-time effect in PWM single-phase inverters produces a distortion that can be expressed as (7) [19], being therefore possible to use any of the high order harmonics in (7) for islanding detection purposes [19].

$$v_{an} = \frac{4\Delta V}{\pi} \sum_{n=1,5,7,\dots} \frac{1}{n} \sin(n\omega_f t) \quad (7)$$

III. Phase-to-phase and phase-to-ground fault detection using pulsating high frequency injection

It has already been mentioned that since islanding in three-phase system occurs simultaneously in all the three phases, it can be readily detected independent of the high frequency signal injection mode, i.e. stationary or rotating. It is noted in this regard that the implementation of the injection in the stationary reference frame is slightly simpler. However, the injection of the high frequency signal in a rotating reference frame opens interesting possibilities for

the detection of phase-to-phase and phase-to-ground faults in three-phase systems.

Fig. 5a and 5b show the PCC voltage vector spectrum in a rotating reference frame (dq_e in Fig. 2) and in a stationary reference frame (idq_s in Fig. 2), when the pulsating high frequency voltage is been superimposed on top of the fundamental excitation. As shown in Fig. 5a, the pulsating high frequency signal can be decomposed in two rotating signals, v_{dqhf}^{pc} and v_{dqhf}^{nc} of frequencies ω_{hf} and $-\omega_{hf}$ respectively. By transforming this voltage vector to the stationary reference frame (see Fig. 5b), the frequency components v_{dqhf}^{pc} and v_{dqhf}^{nc} at $\omega_{hf} + \omega_i$ and $-\omega_{hf} + \omega_i$ are obtained respectively.

The most typical asymmetric faults that occur in three-phase systems are the phase-to-ground, phase-to-phase and phase-to-neutral [21]. Typically the neutral wire is not available in the connection of three-phase distributed energy resources to the utility grid/microgrid through three-phase VSI (see Fig. 1a). Therefore, only the phase-to-ground and phase-to-phase faults will be analyzed in this section.

a) Phase-to-ground fault

When a pulsating voltage vector is injected into a three-phase system with a fault to ground in phase a (see Fig. 6a), the resulting high frequency phase currents are given by (8). The pulsating signal is injected in a dq_e reference frame which rotates at $\omega_i = 50\text{Hz}$ and it is assumed that the fault impedance is much lower than the system (load) impedance (Z_L).

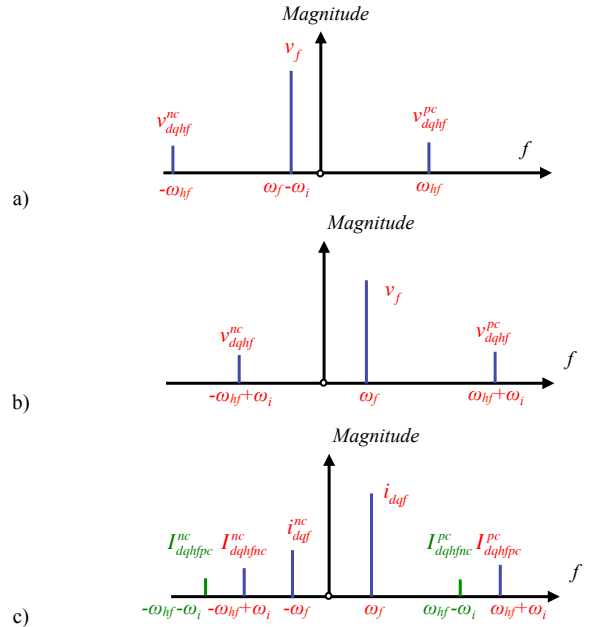


Fig. 5. a) PCC voltage vector spectrum in a rotating reference frame and b) in a stationary reference frame. c) Output inverter current vector spectrum when feeding a non-symmetrical load.

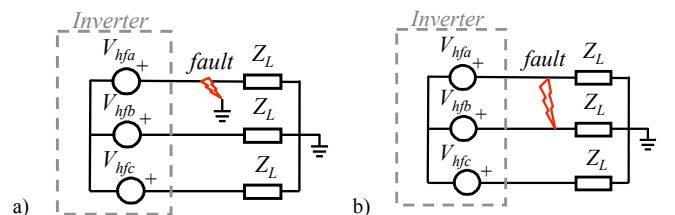


Fig. 6. a) Phase-to-ground fault, and b) phase-to-phase fault.

$$\begin{bmatrix} i_a \\ i_b \\ i_c \end{bmatrix} = \begin{bmatrix} \frac{V_a 3}{Z_L} e^{j((\omega_{hf} + \omega_i)t - \varphi_{Z_L})} \\ \frac{V_b \sqrt{3}}{Z_L} e^{j((\omega_{hf} + \omega_i)t - 5^*\pi/6 - \varphi_{Z_L})} \\ \frac{V_c \sqrt{3}}{Z_L} e^{j((\omega_{hf} + \omega_i)t + 5^*\pi/6 - \varphi_{Z_L})} \end{bmatrix} + \begin{bmatrix} \frac{V_a 3}{Z_L} e^{j((-\omega_{hf} + \omega_i)t + \varphi_{Z_L})} \\ \frac{V_b \sqrt{3}}{Z_L} e^{j((-\omega_{hf} + \omega_i)t + 5^*\pi/6 + \varphi_{Z_L})} \\ \frac{V_c \sqrt{3}}{Z_L} e^{j((-\omega_{hf} + \omega_i)t - 5^*\pi/6 + \varphi_{Z_L})} \end{bmatrix} \quad (8)$$

Applying *Fortescue's* theorem, (9), to the components in (8) at $\omega_{hf} + \omega_i$, a set of symmetrical components is obtained (10), with i_{dqhfpc}^0 , i_{dqhfpc}^{pc} and i_{dqhfpc}^{nc} being the zero, positive and negative sequence components respectively. It is noted that though the same transformation could be used with the components in (9) at $-\omega_{hf} + \omega_i$, the discussion following focuses only for the frequency components at $\omega_{hf} + \omega_i$.

$$\begin{bmatrix} i^0 \\ i^+ \\ i^- \end{bmatrix} = \begin{bmatrix} 1 & 1 & 1 \\ 1 & a & a^2 \\ 1 & a^2 & a \end{bmatrix} * \begin{bmatrix} i_a \\ i_b \\ i_c \end{bmatrix} \quad (9)$$

$$\begin{bmatrix} i_{dqhfpc}^0 \\ i_{dqhfpc}^{pc} \\ i_{dqhfpc}^{nc} \end{bmatrix} = \begin{bmatrix} 0 \\ \frac{2\sqrt{3}}{3} I_{cc} e^{j((\omega_{hf} + \omega_i)t - \varphi_{Z_L})} \\ \frac{\sqrt{3}}{3} I_{cc} e^{j((-\omega_{hf} - \omega_i)t - \varphi_{Z_L})} \end{bmatrix} \quad (10)$$

where $I_{cc} = V_b \sqrt{3} / Z_L$.

If the fault occurs in phase *b*, the resulting symmetrical components using (9) are given by (11), while if the fault occurs in phase *c* it is expressed by (12). It is observed from (10)-(12) that the faulty phase can be detected from the phase angle between the positive sequence component (i_{dqhfpc}^{pc}) and the negative sequence component (i_{dqhfpc}^{nc}), which is θ when the faulty phase is phase *a*, $2\pi/3$ when the faulty phase is phase *b* and $4\pi/3$ when the faulty phase is phase *c*.

$$\begin{bmatrix} i_{dqhfpc}^0 \\ i_{dqhfpc}^{pc} \\ i_{dqhfpc}^{nc} \end{bmatrix} = \begin{bmatrix} 0 \\ \frac{2\sqrt{3}}{3} I_{cc} e^{j((\omega_{hf} + \omega_i)t - \varphi_{Z_L})} \\ \frac{\sqrt{3}}{3} I_{cc} e^{j((-\omega_{hf} - \omega_i)t + 2\pi/3 - \varphi_{Z_L})} \end{bmatrix} \quad (11)$$

$$\begin{bmatrix} i_{dqhfpc}^0 \\ i_{dqhfpc}^{pc} \\ i_{dqhfpc}^{nc} \end{bmatrix} = \begin{bmatrix} 0 \\ \frac{2\sqrt{3}}{3} I_{cc} e^{j((\omega_{hf} + \omega_i)t - \varphi_{Z_L})} \\ \frac{\sqrt{3}}{3} I_{cc} e^{j((-\omega_{hf} - \omega_i)t + 4\pi/3 - \varphi_{Z_L})} \end{bmatrix} \quad (12)$$

b) Phase-to-phase fault

When a pulsating voltage vector which rotates at ω_i , is injected into a three-phase system in which a phase-to-phase fault between phases *a-b* occurs (see Fig. 6b), the resulting phase currents are expressed by (13) and the resulting symmetrical components are given by (14) (only the phasors for the frequency components at $\omega_{hf} + \omega_i$ are shown). It is assumed that the fault impedance (Z_F) is much lower than the load impedance (Z_L).

The resulting symmetrical components when the fault occurs between phases *b-c* or *c-a* are given by (15)-(16). It is observed by comparing (14)-(16) that the faulty phases

can be detected from the phase angle between i_{dqhfpc}^{pc} and i_{dqhfpc}^{nc} . I.e. $\pi/3$ when the fault occurs between phases *a* and *b*, π when the fault occurs between phases *b* and *c* and $-\pi/3$ when the fault occurs between phases *a* and *c*.

$$\begin{bmatrix} i_a \\ i_b \\ i_c \end{bmatrix} = \begin{bmatrix} \frac{V_{ab}}{Z_F} e^{j((\omega_{hf} + \omega_i)t - \pi/6 - \varphi_{Z_F})} \\ -\frac{V_{ab}}{Z_F} e^{j((\omega_{hf} + \omega_i)t - \pi/6 - \varphi_{Z_F})} \\ 0 \end{bmatrix} + \begin{bmatrix} \frac{V_{ab}}{Z_F} e^{j((-\omega_{hf} + \omega_i)t + \pi/6 + \varphi_{Z_F})} \\ \frac{V_{ab}}{Z_F} e^{j((-\omega_{hf} + \omega_i)t + \pi/6 + \varphi_{Z_F})} \\ 0 \end{bmatrix} \quad (13)$$

$$\begin{bmatrix} i_{dqhfpc}^0 \\ i_{dqhfpc}^{pc} \\ i_{dqhfpc}^{nc} \end{bmatrix} = \begin{bmatrix} 0 \\ \frac{\sqrt{3}}{3} I_{cc} e^{j((\omega_{hf} + \omega_i)t - \varphi_{Z_F})} \\ \frac{\sqrt{3}}{3} I_{cc} e^{j((-\omega_{hf} - \omega_i)t + \pi/3 - \varphi_{Z_F})} \end{bmatrix} \quad (14)$$

$$\begin{bmatrix} i_{dqhfpc}^0 \\ i_{dqhfpc}^{pc} \\ i_{dqhfpc}^{nc} \end{bmatrix} = \begin{bmatrix} 0 \\ \frac{\sqrt{3}}{3} I_{cc} e^{j((\omega_{hf} + \omega_i)t - \varphi_{Z_F})} \\ \frac{\sqrt{3}}{3} I_{cc} e^{j((\omega_{hf} + \omega_i)t + \pi - \varphi_{Z_F})} \end{bmatrix} \quad (15)$$

$$\begin{bmatrix} i_{dqhfpc}^0 \\ i_{dqhfpc}^{pc} \\ i_{dqhfpc}^{nc} \end{bmatrix} = \begin{bmatrix} 0 \\ \frac{\sqrt{3}}{3} I_{cc} e^{j((\omega_{hf} + \omega_i)t - \varphi_{Z_F})} \\ \frac{\sqrt{3}}{3} I_{cc} e^{j((\omega_{hf} + \omega_i)t - \pi/3 - \varphi_{Z_F})} \end{bmatrix} \quad (16)$$

where $I_{cc} = V_{ab} / Z_F$.

IV. Simulation results

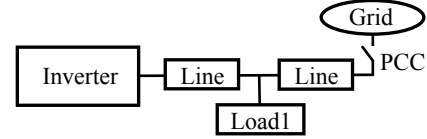


Fig. 5. Simulation scenario for both three and single-phase systems

Fig. 5 shows the scenario used to simulate the proposed islanding and fault detection methods. The same scenario was used for both single-phase and three-phase cases, the corresponding inverter topologies being shown in Fig. 1. The simulation parameters are shown in Table I.

Table I			
Three phase			
Grid	Inverter	Load	Line
380V, 50 Hz, $r_g/X_g=0.1$, $S_{cc}=15MVA$	380V, 10kHz	3 kW	R=11.7mOhm L=8.68e-4H
Single phase			
Grid	Inverter	Load	Line
220V, 50 Hz, $r_g/X_g=0.1$, $S_{cc}=5MVA$	220V, 10kHz	1 kW	R=11.7mOhm L=8.68e-4H

a) Islanding detection

Fig. 6 shows a transition from island to grid connected for the case of a three-phase system, when the pulsating high frequency signal is injected in a stationary reference frame (dq_s , see Fig. 3). Fig. 6a shows the dq_s components of the filter output voltage and Fig. 6b shows the dq_s components of the inverter output current; Both the voltages and currents

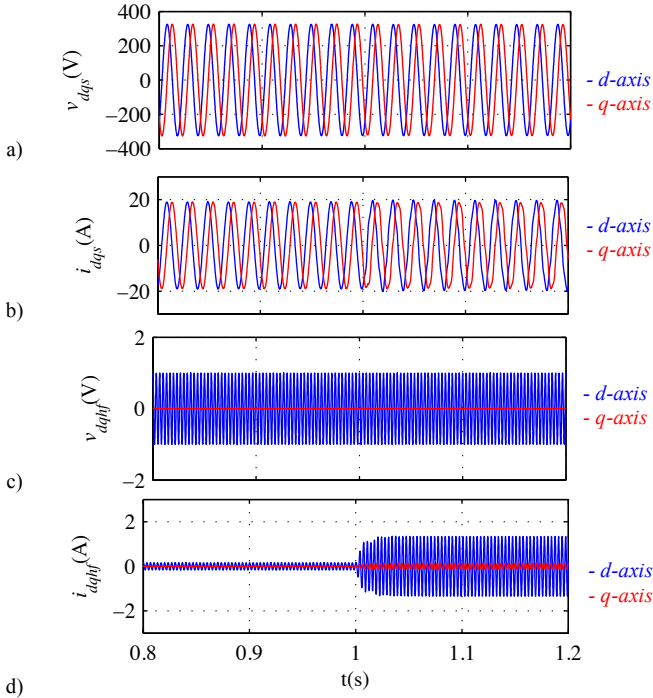


Fig. 6 Simulation results. Transition from island to grid connected ($t=1$ s) for the case of three-phase system. a) dq_s components of the filter output voltages, b) dq_s components of the inverter output currents, c) dq_s components of the injected high frequency voltages and d) dq_s components of the inverter high frequency currents. $\omega_{hf}=300$ Hz, $V_{hf}=0.01$ pu.

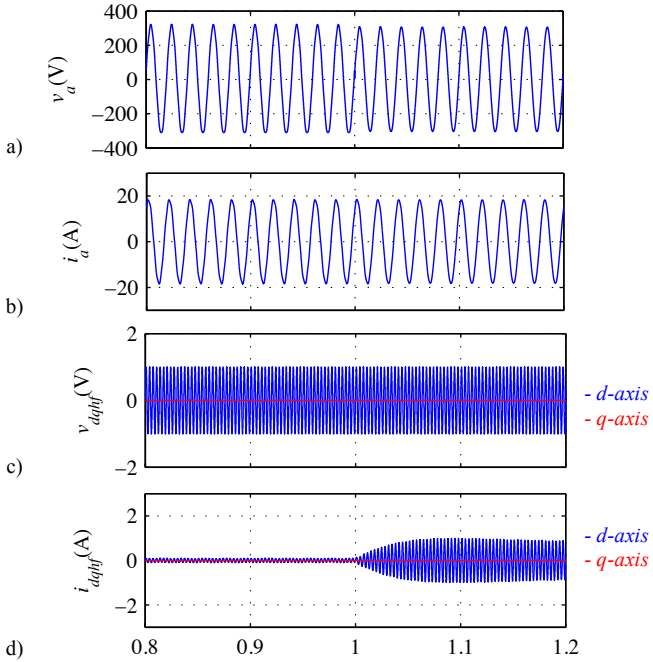


Fig. 7 Simulation results. Transition from island to grid connected ($t=1$ s), for the case of a single-phase system. a) Filter output voltage, b) inverter output current, c) dq_s components of the injected high frequency voltages, and d) dq_s components of the inverter high frequency currents. $\omega_{hf}=300$ Hz, $V_{hf}=0.01$ pu.

shown in Fig. 6a and 6b consist of the fundamental component and the high frequency component, the latest being practically imperceptible due to its reduced amplitude. Fig. 6c shows the dq_s components of the injected inverter high frequency voltage after removing the fundamental voltage. Similarly, Fig 6d shows the high frequency components of the inverter output current once the

fundamental current has been removed. An increase of the high frequency current magnitude is readily observed after the transition from island to grid connected condition, due to the reduction of the overall high frequency impedance.

Fig. 7 shows the same simulation results as in Fig. 6 for the case of a single-phase system. Fig. 7a and 7b show the inverter output voltage and current respectively (fundamental and high frequency components), while Fig. 7c and 7d shows the corresponding high frequency components. A similar behavior of the inverter output high frequency current is observed, the transition between grid and island modes being readily observed.

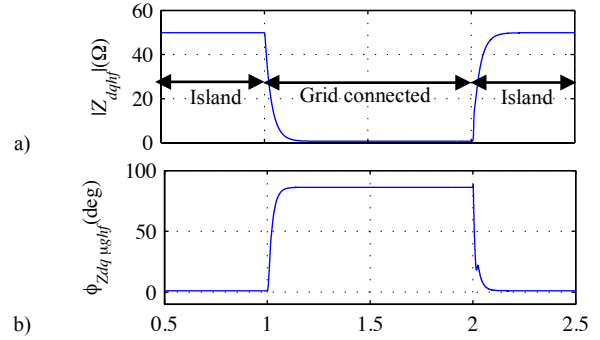


Fig. 8 Simulation results. a) Estimated high frequency impedance magnitude and b) phase for the case of a three-phase system. Stationary reference frame high frequency signal injection. $\omega_{hf}=300$ Hz, $V_{hf}=0.01$ pu.

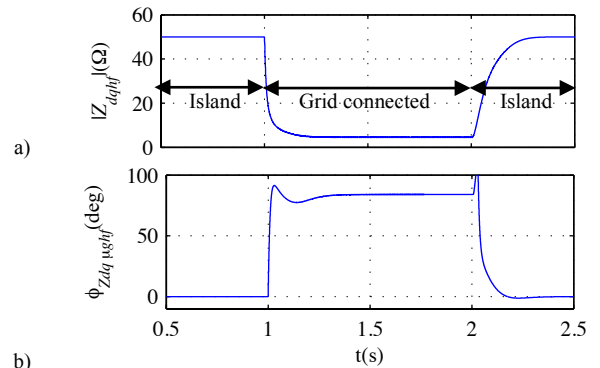


Fig. 9 Simulation results. a) Estimated high frequency impedance magnitude and b) phase, for the case of single-phase system. $\omega_{hf}=300$ Hz, $V_{hf}=0.01$ pu.

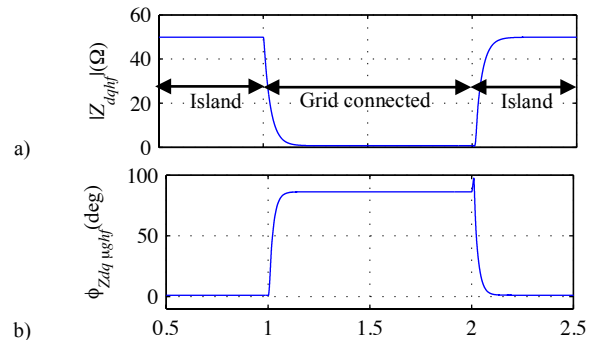


Fig. 10 Simulation results. a) Estimated high frequency impedance magnitude and b) phase for the case of a three-phase system when the pulsating high frequency signal is injected in a rotating reference frame. $\omega_r=50$ Hz, $\omega_{hf}=300$ Hz, $V_{hf}=0.01$ pu.

Fig. 8 and 9 show the estimated high frequency impedance for three-phase and single-phase systems respectively, when transitions from island to grid and from grid to island occur at $t=1$ s and $t=2$ s. It is observed that the estimated high frequency impedance is available in a few

ms., meeting therefore the islanding detection standards [1-8].

As already mentioned, the pulsating high frequency signal can be injected either in a stationary or a rotating reference frame in three phase systems. This is confirmed by the results shown in Fig. 10 where grid-island and grid-island transitions are readily observed in the high frequency impedance when the high frequency signal is injected in a rotating reference frame.

c) Fault detection

Fig. 11a and 11b show the magnitude of i_{dqhfpc}^{nc} and the phase angle between i_{dqhfpc}^{pc} and i_{dqhfpc}^{nc} , for the following faults: phase-to-ground faults in phase a ($0.5 < t < 1$ s), b ($1 < t < 1.5$ s) and c ($1.5 < t < 2$ s), and phase-to-phase faults between phases a - b ($2 < t < 2.5$ s) and b - c ($2.5 < t < 3$ s). It is observed that the magnitude of i_{dqhfpc}^{nc} is zero when there is no fault, the type (phase-to-ground or phase-to-phase) and location of the fault being detected from the phase angle between i_{dqhfpc}^{pc} and i_{dqhfpc}^{nc} .

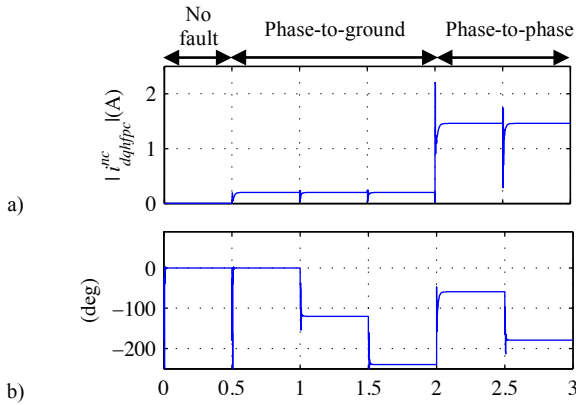


Fig. 11 Simulation results. a) i_{dqhfpc}^{nc} magnitude and b) phase angle between i_{dqhfpc}^{pc} and i_{dqhfpc}^{nc} for the case of a phase-to-ground fault in phase a ($0.5 < t < 1$ s), b ($1 < t < 1.5$ s) and c ($1.5 < t < 2$ s), and for the case of a phase-to-phase fault between phases a - b ($2 < t < 2.5$ s) and b - c ($2.5 < t < 3$ s). $\omega_r=50$ Hz, $\omega_{hf}=300$ Hz, $V_{hf}=0.01$ pu.

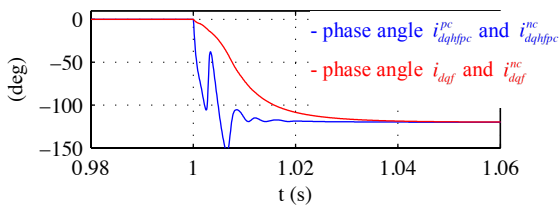


Fig. 12 Simulation results. Phase angle between i_{dqhfpc}^{pc} and i_{dqhfpc}^{nc} and between i_{daf} and i_{daf}^{nc} . $\omega_r=50$ Hz, $\omega_{hf}=300$ Hz, $V_{hf}=0.01$ pu.

Finally, Fig. 12 shows the dynamic behavior of the angle between positive and negative components of the high frequency current, i_{dqhfpc}^{pc} and i_{dqhfpc}^{nc} (blue), as well as between the positive and negative components of the fundamental current, i_{daf} and i_{daf}^{nc} (red), when a phase-to-ground fault occurs in phase b ($t=1$ s). It is observed that the phase angle between high frequency signals (i.e. i_{dqhfpc}^{pc} and i_{dqhfpc}^{nc}) has a faster transient response than that of the fundamental components (i.e. i_{daf} and i_{daf}^{nc}), therefore enabling faster fault detection.

V. Experimental results

Fig. 13 shows the experimental setup used both for the case of a three-phase and a single-phase systems. The parameters are shown in Table II.

Table I			
Three phase			
Grid	Inverter	Load	Line
380V, 50 Hz, $r_g/X_g=0.1$, $S_{cc}=15$ MVA	380V, 10kHz	3 kW	R=0.1Ohm
Single phase			
Grid	Inverter	Load	Line
220V, 50 Hz, $r_g/X_g=0.1$, $S_{cc}=5$ MVA	220V, 10kHz	2 kW	R=0.1Ohm

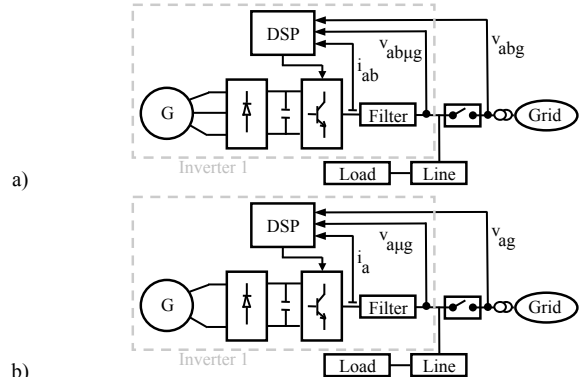


Fig. 13 Experimental setup. a) Three-phase, b) single-phase.

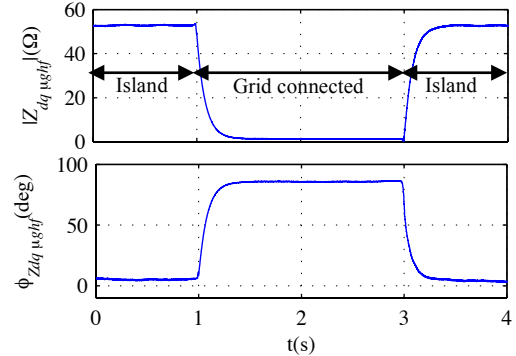


Fig. 14 a) Estimated high frequency impedance magnitude and b) phase when the pulsating high frequency signal is injected in the stationary reference frame. $\omega_{hf}=300$ Hz, $V_{hf}=0.01$ pu.

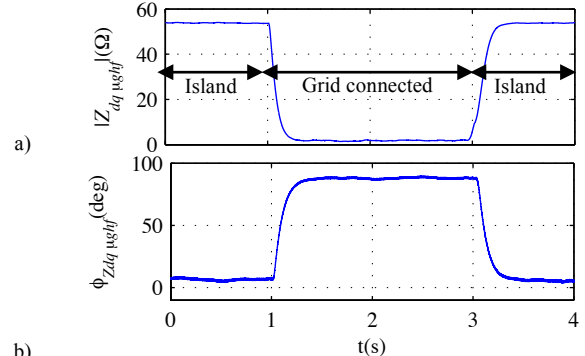


Fig. 15 a) Estimated high frequency impedance magnitude, and b) phase when the pulsating high frequency signal is injected in a rotating reference frame. $\omega_r=50$ Hz, $\omega_{hf}=300$ Hz, $V_{hf}=0.01$ pu.

Fig. 14, 15 and 16 show the magnitude and phase of the estimated high frequency impedance during a transition for island to grid-connected ($t=1$ s) and from grid-connected to island ($t=3$ s). The high frequency signal was injected in the

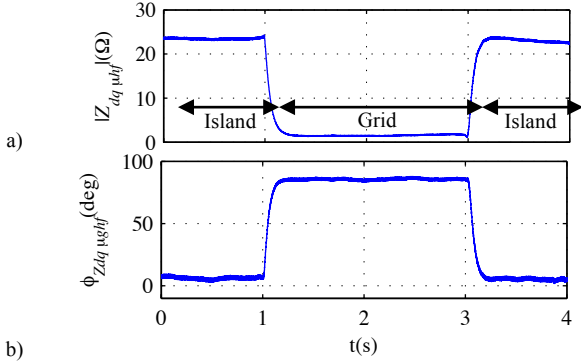


Fig. 16 a) Estimated high frequency impedance magnitude and b) phase. Single-phase system. $\omega_{hf}=300$ Hz, $V_{hf}=0.01$ pu.

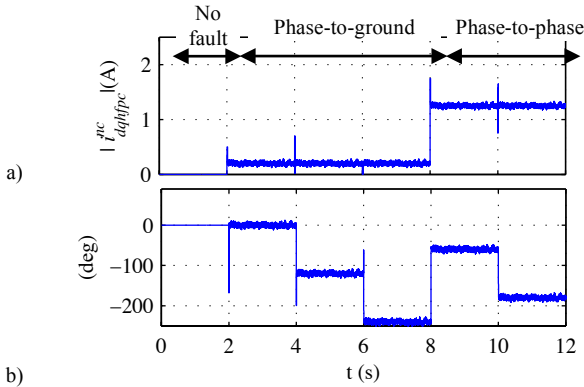


Fig. 17 a) i_{dqhf}^{nc} magnitude and b) phase angle between i_{dqhf}^{pc} and i_{dqhf}^{nc} for the case of a phase-to-ground fault in phase a ($2 < t < 4$ s), b ($4 < t < 6$ s) and c ($6 < t < 8$ s), and for the case of a phase-to-phase fault between phases a - b ($8 < t < 10$ s) and b - c ($10 < t < 12$ s). $\omega_i=50$ Hz, $\omega_{hf}=300$ Hz, $V_{hf}=0.01$ pu.

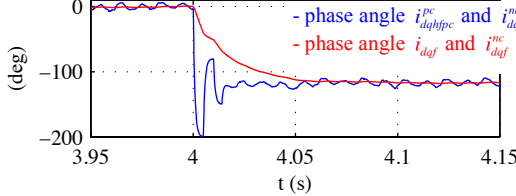


Fig. 18 Phase angle between i_{dqhf}^{pc} and i_{dqhf}^{nc} (blue) and between i_{daf} and i_{daf}^{nc} (red) respectively. $\omega_i=50$ Hz, $\omega_{hf}=300$ Hz, $V_{hf}=0.01$ pu.

stationary reference frame in Fig. 14 and in a rotating reference frame in Fig. 15. It is observed that the high frequency impedance change is detected after a few ms both for the case of three-phase and single-phase systems, therefore meeting the islanding detection standards [1-8].

Fig. 11a and 11b show the magnitude of i_{dqhf}^{nc} and the phase angle between i_{dqhf}^{pc} and i_{dqhf}^{nc} , for the following faults: phase-to-ground faults in phase a ($2 < t < 4$ s), b ($4 < t < 6$ s) and c ($6 < t < 8$ s), and phase-to-phase faults between phases a - b ($8 < t < 10$ s) and b - c ($10 < t < 12$ s). It is observed that the magnitude of i_{dqhf}^{nc} is zero when there is no fault, the type of fault being readily detected from the phase angle between i_{dqhf}^{pc} and i_{dqhf}^{nc} . Finally Fig. 18 shows the transient behavior of the phase angle between i_{dqhf}^{pc} and i_{dqhf}^{nc} (blue) and between i_{daf} and i_{daf}^{nc} (red), when a phase-to-ground fault occurs in phase b ($t=4$ s) (see description for Fig. 12). In all the cases, it is observed a remarkable agreement with the simulation results shown in Section IV.

VI. Conclusions

This paper proposes an islanding detection method based on the injection of a pulsating high frequency signal. The

method is suitable both for three-phase and single-phase systems. This is an advantage compared to most of already proposed active islanding detection methods based on the impedance estimation variation by means of a high frequency signal injection [9, 17-18].

The island/grid-connected condition is detected in a few ms in both three-phase and single-phase systems, which is fast enough to meet the islanding detection standards [1-8].

It has been also shown that injection of a pulsating high frequency signal can be additionally used for unbalance fault detection in three-phase system.

Simulation and experimental results have been provided to confirm the viability of both proposed methods: islanding and unbalanced fault detection.

VII. References

- [1] IEEE, "IEEE Standard for Interconnecting distributed resources with electric power systems," IEEE Std. 1547, 2003.
- [2] UL1741, *UL Standard for Safety for Static Converters and Charge Controllers for Use in Photovoltaic Power Systems*, Underwriters Laboratories, May 7, 1999, revised June 2001.
- [3] IEC 62116, Testing Procedure of Islanding Prevention Measures for Grid Connected Photovoltaic Power Generation Systems, International Electrotechnical Commission.
- [4] Australian Standard AS4777, "Grid Connection Of Energy Systems Via Inverters Part 3: Grid Protection Requirements".
- [5] IEEE Std. 929-2000, IEEE Recommended Practice for Utility Interface of Photovoltaic (PV) Systems, IEEE Standards Coordinating Committee 21 on Photovoltaics, New York, NY, Apr. 2000.
- [6] DIN-VDE, "Automatic Disconnection Device Between a Generator and the Low-Voltage Grid," DIN-VDE Std. 0126-1-1, 2005.
- [7] ÖVE/Önorm E 2750 "Photovoltaische Energieerzeugungsanlagen – Sicherheitsanforderungen ("Photovoltaic power generating systems – safety requirements").
- [8] VSE Sonderdruck Abschnitt 12 'Werkvorschriften über die Erstellung von elektr. Installation' Elektrische Energieerzeugungsanlagen Completes VSE 2.8d-95.
- [9] F. Briz, D. Reigosa, C. Blanco and J.M. Guerrero, "Coordinated operation of parallel-connected inverters for active islanding detection using high frequency signal injection" IEEE Trans. on Ind. Appl., accepted 2014.
- [10] A. Timbus, A. Oudalov, C. N.M. Ho, "Islanding Detection in Smart Grids," IEEE-ECCE'10, pp.3631 – 3637, Sep. 2010.
- [11] R. Teodorescu, M. Liserre, P. Rodriguez and F. Blaabjerg, *Grid Converters for Photovoltaic and Wind Power Systems*, Wiley-IEEE 2011.
- [12] M. Ciobotaru, R. Teodorescu, P. Rodriguez, A. Timbus and F. Blaabjerg, "On-line Grid Impedance Estimation for Single Phase Grid-Connected Systems Using PQ Variations", IEEE-PESC, pp.2306–2312, June 2007.
- [13] A. V. Timbus, R. Teodorescu and U. Borup, "Online Grid Impedance Measurement Suitable for Multiple PV Inverters Running in Parallel", IEEE-APEC'06, pp.907–911, March 2006.
- [14] L. Asiminoaei, R. Teodorescu, F. Blaabjerg and U. Borup, "A Digital Controlled PV-Inverter with Grid Impedance Estimation for ENS Detection", IEEE Trans. on Ind. Appl., 20(6):1480–1490, Nov.-Dec. 2005.
- [15] L. Asiminoaei, R. Teodorescu, F. Blaabjerg and U. Borup, "A New Method of On-Line Grid Impedance Estimation for PV Inverter", IEEE-APEC'04, pp.1527–1533, Sept. 2004.
- [16] M. Ciobotaru, R. Teodorescu and F. Blaabjerg, "On-line Grid Impedance Estimation Based on Harmonic Injection for Grid-Connected PV Inverter", IEEE-ISIE, pp.2473–2442, June 2007.
- [17] D. Reigosa, F. Briz, C. Blanco, P. Garcia and J. M. Guerrero, "Active Islanding Detection Using High Frequency Signal Injection", IEEE Trans. on Ind. Appl., 48(5):1588–1597, Sept. 2012.
- [18] D. Reigosa, F. Briz, C. Blanco, P. Garcia and J. M. Guerrero, "Active Islanding Detection for Multiple Parallel-Connected Inverter-Based Distributed Generators Using High Frequency Signal Injection," IEEE Trans. on Power Elect., 49(3):1411–1420, March 2014.
- [19] D. Reigosa, F. Briz, C. Blanco and J. M. Guerrero, "Islanding detection in grid-connected power converters using harmonics due to the non-ideal behavior of the inverter," IEEE-ECCE'13, pp. 2649–2656, Sept. 2013.
- [20] Y. Xue, L. Chang, S.B. Kjaer, J. Bordonau and T. Shimizu, "Topologies of Single-Phase Inverters for Small Distributed Power Generation: An Overview," IEEE Trans. on Power Elect., 15(5):1305–1314, Sept. 2004.
- [21] A. A. Sallam and OM P. Malik, "Electric Distribution Systems," Wiley-IEEE 2011.